Cover Page

Universiteit Leiden

The handle http://hdl.handle.net/1887/25979 holds various files of this Leiden University dissertation

Author: Boon, Mariëtte
Title: Turning up the heat : role of brown adipose tissue in metabolic disease
Issue Date: 2014-06-12

CANNABINOID 1 RECEPTOR BLOCKADE DIMINISHES OBESITY AND DYSLIPIDEMIA VIA PERIPHERAL ACTIVATION OF BROWN ADIPOSE TISSUE

MARIËTTE R. BOON
SANDER KOOIJMAN
ANDREA D. VAN DAM
LEONARD R. PELGROM
JIMMY F.P. BERBÉE
CHERYL A.R. VISSEREN
ROBIN C. VAN AGGELE
ANITA M. VAN DEN HOEK
HETTY C.M. SIPS
MARC LOMBÈS
LOUIS M. HAVEKES
JOUKE T. TAMSMA
BRUNO GUIGAS
ONNO C. MEIJER
J. WOUTER JUKEMA
PATRICK C.N. RENSEN

ABBREVATIONS

ACC2	acetyl-CoA carboxylase 2
ACSL1	long-chain-fatty-acid-CoA ligase 1
BAT	brown adipose tissue
CB1R	cannabinoid type 1 receptor
CHO	carbohydrate
DIO	diet-induced obesity
E3L.CETP	APOE*3-Leiden.CETP
FASN	fatty acid synthase
(F)FA	(free) fatty acids
HSL	hormone-sensitive lipase
LPL	lipoprotein lipase
PL	phospholipids
SCD-1	stearoyl-CoA desaturase
TC	total cholesterol
TG	triglyceride
UCP-1	uncoupling protein-1
SNS	sympathetic nervous system
VLDL	very-low density lipoprotein
(g,s)WAT	(gonadal, subcutaneous) white adipose tissue

ABSTRACT

The endocannabinoid system is an important player in energy metabolism by regulating appetite, lipolysis and energy expenditure. Chronic blockade of the cannabinoid 1 receptor (CB1R) leads to long-term maintained weight loss and reduction of dyslipidemia in experimental and human obesity. The molecular mechanism by which CB1R blockade reverses dyslipidemia in obesity has not been clarified yet. In this study, we show that systemic CB1R blockade by rimonabant in a diet-induced obese mouse model for human-like lipoprotein metabolism reversed obesity, increased energy expenditure and lowered plasma VLDL-triglycerides (TG). Mechanistic studies showed that rimonabant selectively increased VLDL-TG clearance by brown adipose tissue (BAT) accompanied by decreased lipid droplet size in BAT. Of note, the mechanism involved peripheral activation of BAT since the effects were still present at thermoneutral temperature at which sympathetic output towards BAT is negligible and could be fully recapitulated by using the strictly peripheral CB1R antagonist AM6545. In support, we demonstrate that the CB1R is highly expressed in BAT and that *in vitro* blockade of the CB1R in cultured brown adipocytes increased UCP-1 content and lipolysis. Our data indicate that selective targeting of the peripheral CB1R in BAT has therapeutic potential in attenuating dyslipidemia and obesity.

7

INTRODUCTION

The endocannabinoid system regulates a broad range of physiological functions (1) and consists of G-protein coupled cannabinoid receptors, its endogenous lipid ligands (endocannabinoids) and the enzymes involved in the biosynthesis and degradation of endocannabinoids (2,3). The cannabinoid type 1 receptor (CB1R) is expressed at high levels in the brain but also at functionally relevant concentrations in various peripheral tissues (1). In contrast, the cannabinoid type 2 receptor is mainly expressed on immune cells (4). CB1R knockout mice display reduced adiposity and are resistant to diet-induced obesity (5). Moreover, overweight and obese humans exhibit an overactive endocannabinoid system (6,7), suggesting a role of the endocannabinoid system in energy metabolism.

Chronic systemic blockade of the CB1R with the inverse agonist rimonabant leads to long-term maintained weight loss and reduction of dyslipidemia in obese rodents (8,9) and humans (10-13). Rimonabant was considered one of the most promising therapeutic drugs to treat obesity, until the appearance of central psychiatric side effects resulted in its removal from the market in 2008. Nevertheless, several lines of evidence indicate that the effect of CB1R blockade is not restricted to a central mode of action, especially since the CB1R has been shown to be present in peripheral tissues including the liver (14), skeletal muscle (15) and adipocytes (16). More specifically, Tam et al (17) recently showed that the strictly peripheral CB1R antagonist AM6545 induced weight loss and diminished hepatic steatosis in a mouse model. Thus, it seems plausible that psychiatric side effects can be avoided by strict peripheral blockade of the CB1R, while retaining the beneficial anti-obesity and lipid-lowering effects.

Despite clear evidence that pharmacological CB1R antagonism improves dyslipidemia, the exact mechanisms and the peripheral tissues involved have not yet been elucidated. Recently, brown adipose tissue (BAT) emerged as an important player in triglyceride (TG) clearance (18). In contrast to white adipose tissue (WAT), which stores excess TG as fat, BAT dissipates energy into heat, a process mediated by the mitochondrial uncoupling protein-1 (UCP-1) (19). The best known trigger for activation of BAT is cold, which increases sympathetic outflow from the hypothalamic temperature centre towards BAT, leading to release of noradrenalin and increased thermogenesis (19). Metabolically active BAT stores exist in adult humans (20-22), and BAT volume and activity are lower in obese subjects (22). In addition, BAT volume and activity are lower in South Asians, a population prone to develop type 2 diabetes mellitus and cardiovascular disease (23). Together, these findings have increased interest in the therapeutic potential of BAT to combat obesity and related disorders, such as dyslipidemia.

In this study, we aimed at elucidating the molecular mechanism by which CB1R blockade attenuates dyslipidemia in diet-induced obesity by using a mouse model for human-like lipoprotein metabolism.

MATERIALS AND METHODS

Animals and diet

Homozygous human cholesteryl ester transfer protein (CETP) transgenic mice were crossbred with hemizygous APOE*3-Leiden (E3L) mice at our Institutional Animal Facility to obtain E3L. CETP mice, as previously described (24). We chose to perform our studies in this specific mouse model, since these mice are a well-established model for human-like lipoprotein metabolism and respond to lipid-lowering pharmacological interventions (24-26). In all the studies described below, 10 week-old E3L.CETP male mice were housed under standard conditions in conventional cages in a 12:12 h light: dark cycle with *ad libitum* access to food and water, and were fed a high-fat diet (HFD; Research diets, New Brunswick, USA, 60% lard fat) for 12 weeks to induce obesity. From the 7th week onwards, the drinking water was supplied with 10% fructose. All mouse experiments were performed in accordance with the Institute for Laboratory Animal Research Guide for the Care and Use of Laboratory Animals and have received approval from the Departmental Ethical Review Board (Leiden University Medical Center, Leiden, The Netherlands).

Pharmacological intervention

After 12 weeks of HFD, diet-induced obese (DIO) mice were randomised according to their body weight and plasma total cholesterol (TC) and triglyceride (TG) levels into four groups. Subsequently, mice were housed at either 21°C (subthermoneutral) or 28°C (thermoneutral), and received 60% HFD with or without 10 mg/kg body weight/day (0.00885%, w/w) rimonabant (Axon Medchem, Groningen, the Netherlands) or AM6545 (Sigma-Aldrich, St. Louis, USA) for 4 weeks.

Body weight and food intake

In all experiments, mice were housed individually during the 4 week treatment period. Food intake was recorded daily by weighing the food that was left in the cage or was recorded automatically in metabolic cages (see below). Body weight was measured twice a week.

Indirect calorimetry and physical activity

Indirect calorimetry was performed in fully automatic metabolic cages (LabMaster System, TSE Systems, Bad Homburg, Germany) during the fourth week of treatment. After 20 h acclimatization, oxygen uptake ($\dot{V} O_2$), carbon dioxide production ($\dot{V} CO_2$) and caloric intake were measured for 5 consecutive days. Carbohydrate (CHO) and fat oxidation rates were calculated from $\dot{V} O_2$ and $\dot{V} CO_2$ as described previously (27). Total energy expenditure (EE) was calculated from $\dot{V} O_2$ and $\dot{V} CO_2$ using the Weir equation (28). Physical activity was measured using infrared sensor frames.

Dual-energy X-ray absorptiometry (DEXA) scan

After 4 weeks treatment, body composition was measured by DEXA using the Norland pDEXA Sabre X-ray Bone Densitometer. Mice were anaesthetized intraperitoneally with a

combination of 6.25 mg/kg acepromazine (Alfasan), 6.25 mg/kg midazolam (Roche) and 0.31 mg/kg fentanyl (Janssen-Cilag). The total body of the mice was scanned, yet the heads were excluded from the analyses.

Plasma parameters

Blood was collected from the tail vein of 4-6 hour fasted mice into chilled capillaries that were coated with paraoxon (Sigma, St. Louis, MO) to prevent ongoing lipolysis (29). Capillaries were placed on ice and centrifuged, and plasma was assayed for TG, TC, and phospholipids (PL) using commercially available enzymatic kits from Roche Diagnostics (Mannheim, Germany for TG and TC) and Instruchemie (Delfzijl, the Netherlands for PL). Free fatty acids (FFA) were measured using NEFA C kit from Wako Diagnostics (Instruchemie, Delfzijl, The Netherlands).

Lipoprotein profiles

To determine lipid distribution over plasma lipoproteins, pooled plasma was used for fast performance liquid chromatography (FPLC). Plasma was injected onto a Superose 6 column (ÄKTA System, Amersham Pharmacia Biotech, Piscataway, NJ) and eluted at a constant flow rate of 50 μL/min with PBS pH 7.4. TG and TC were measured as described above in collected fractions of 50 μL.

In vivo clearance of labeled VLDL-like emulsion particles

VLDL-like TG-rich emulsion particles (80 nm) labeled with glycerol tri[3H]oleate (triolein, TO) were prepared and characterized as described previously (30). To study the *in vivo* clearance of the VLDL-like particles, mice were fasted for 4 h and injected (t = 0) via the tail vein with 200 μL of emulsion particles (1.0 mg TG per mouse). Blood samples were taken from the tail vein at 2, 10, 20 and 30 min after injection to determine the serum decay of [3H]TO. Plasma volumes were calculated as $0.04706 \times$ body weight (g) as determined from ^{125}I-BSA clearance studies as described previously (31). After taking the last blood sample, mice were cervically dislocated and perfused with ice-cold PBS via the heart to remove blood from the organs. Subsequently, the liver, heart, spleen, hindlimb muscle, gonadal WAT (gWAT), subcutaneous WAT (sWAT) and brown adipose tissue (BAT) were collected. Organs were dissolved overnight at 60°C in Tissue Solubilizer (Amersham Biosciences, Rosendaal, The Netherlands), and 3H activity was quantified. Uptake of [3H]TO-derived radioactivity by the organs was expressed per gram wet tissue weight.

In vivo hepatic VLDL-TG and VLDL-apoB production

To measure VLDL production *in vivo,* mice were fasted for 4 h and anesthetized by intra-peritoneal injection of 6.25 mg/kg acepromazine (Alfasan), 6.25 mg/kg midazolam (Roche) and 0.31 mg/kg fentanyl (Janssen-Cilag). Mice were injected intravenously with Tran[35S] label (150 μCi/mouse) (MP Biomedicals, Eindhoven, The Netherlands) to label newly produced apolipoprotein B (apoB). After 30 min, at t=0 min, Triton WR-1339 (Sigma-Aldrich) was injected intravenously (0.5 mg/g body weight, 10% solution in PBS) to block serum

VLDL-TG clearance. Blood samples were drawn before (t = 0) and at 15, 30, 60, and 90 min after injection of Triton WR-1339 and used for determination of plasma TG concentration as described above. After 90 min, mice were exsanguinated via the retro-orbital plexus. VLDL was isolated from serum after density gradient ultracentrifugation at d<1.006 g/mL by aspiration (32) and examined for incorporated ^{35}S-activity.

RNA isolation and qRT-PCR analysis

Total RNA was isolated with the Nucleospin® RNA II Kit (Macherey-Nagel) according to the manufacturer's instructions. 1 µg of total RNA was reverse-transcribed with iScript cDNA synthesis kit (Bio-Rad), and the obtained cDNA was purified with Nucleospin Extract II kit (Macherey-Nagel). Real-time PCR was carried out on the IQ5 PCR machine (Bio-Rad) using the Sensimix SYBR Green RT-PCR mix (Quantace). Melt curve analysis was included to assure a single PCR product was formed. Expression levels were normalized using glyceraldehyde-3-phosphate dehydrogenase *(Gapdh)*, *ß2-microglobulin* and *36b4* as housekeeping genes. Primer sequences are listed in **TABLE 1.**

Histology

Interscapular BAT, liver and sWAT were removed and fixed directly in 4% paraformaldehyde, dehydrated and embedded in paraffin. For UCP-1 staining in BAT, sections (5 µm) were dewaxed in xylene, rehydrated in ethanol and treated with 3% H_2O_2 (Sigma) in absolute methanol for 30 min. Next, sections were immersed in 10 mmol/L citrate buffer (pH 6.0), boiled for 10 min and cooled down at room temperature. Slides were blocked during 60 min with normal goat serum (1:75 in PBS) and incubated overnight at 4°C with rabbit monoclonal anti-UCP-1 antibodies (Abcam) diluted 1:400 in normal goat serum (1:75). Next, sections

TABLE 1 - **List of primer sequences for RT-PCR**

Gene	Forward primer	Reverse primer
36b4	GGACCCGAGAAGACCTCCTT	GCACATCACTCAGAATTTCAATGG
Acc2	AGATGGCCGATCAGTACGTC	GGGGACCTAGGAAAGCAATC
Acsl1	TGCCAGAGCTGATTGACATTC	GGCATACCAGAAGGTGGTGAG
Atgl	ACAGTGTCCCCATTCTCAGG	TTGGTTCAGTAGGCCATTCC
ß2-microglobulin	TGACCGGCTTGTATGCTATC	CAGTGTGAGCCAGGATATAG
Cd36	GCAAAGAACAGCAGCAAAATC	CAGTGAAGGCTCAAAGATGG
Fasn	GCGCTCCTCGCTTGTCGTCT	TAGAGCCCAGCCTTCCATCTCCTG
Hsl	AGACACCAGCCAACGGATAC	ATCACCCTCGAAGAAGAGCA
Lpl	CCCTAAGGACCCCTGAAGAC	GGCCCGATACAACCAGTCTA
Pgc1a	TGCTAGCGGTTCTCACAGAG	AGTGCTAAGACCGCTGCATT
Prdm16	ACTTTGGATGGGAGCAGATG	CTCCAGGCTCGATGTCCTTA
Scd1	GCGATACACTCTGGTGCTCA	CCCAGGGAAACCAGGATATT
Ucp1	TCAGGATTGGCCTCTACGAC	TGCATTCTGACCTTCACGAC

were incubated for 60 min with biotinylated goat α-rabbit secondary antibodies (Vector Labs) diluted 1:600 in normal goat serum (1:75). Immunostaining was amplified using Vector Laboratories Elite ABC kit (Vector Labs) and the immunoperoxidase complex was visualized with Nova Red (Vector Labs). Counterstaining was performed with Mayer's hematoxylin (1:4). Haematoxylin and Eosin stainings of liver and sWAT sections were done using standard protocols. Intracellular lipid content in BAT was quantified by use of ImageJ (version 1.47).

Liver lipid extraction

Lipids were extracted from livers consistent with a modified protocol from Bligh and Dyer (33). Small liver samples (approx. 50 mg) were homogenized in 10 μL of ice-cold methanol per mg tissue. Lipids were extracted into an organic phase by adding 1800 μL of CH_3OH: $CHCl_3$ (3:1, vol/vol) to 45 μL of homogenate and subsequent centrifugation. The lower, organic phase was dried and suspended in 2% Triton X-100. Hepatic TG and TC concentrations were measured using commercial kits, as explained (see: *Plasma parameters*). Liver lipids were expressed per milligram of protein, which was determined using the BCA protein assay kit (Thermo Scientific, Rockford, IL, USA).

In vitro experiments with brown adipocytes

The murine brown preadipocyte cell line T37i (34) was cultured in HAM'S-F12 medium (Gibco-Invitrogen) supplemented with 10% fetal calf serum, 2 mM HEPES, 100 U/mL penicillin and 100 μg/mL streptomycin (Gibco-Invitrogen). For experiments, T37i cells were seeded in 6-wells plates and grown towards confluence. Two days after reaching confluence, cells were differentiated using normal culture medium supplemented with 2 nM triiodothyronine (T3) (Sigma) and 112 ng/mL bovine insulin (Sigma). The differentiation medium was replaced every 2 or 3 days. After 9 days of differentiation, cells were stimulated for 8 h with rimonabant (Axon Medchem) at 0.1 μM or 1 μM or with vehicle (DMSO). Then, 500 μL of supernatant was collected and snap-frozen in liquid nitrogen. Cells were washed twice with ice-cold PBS and cells were harvested in ice-cold lysis buffer as described below.

Protein isolation and Western Blot

T37i cells or snap-frozen tissue samples were lysed in ice-cold buffer containing 50 mM Hepes (pH 7.6), 50 mM NaF, 50 mM KCl, 5 mM NaPPi, 1 mM EDTA, 1 mM EGTA, 1 mM DTT, 5 mM ß-glycerophosphate, 1 mM sodium vanadate, 1% NP40 and protease inhibitors using cocktail tablets (Roche). Homogenates were centrifuged at 13,000 rpm for 15 min at 4°C and the protein content of the supernatant was determined using the BCA Protein Assay Kit from Thermo Scientific. Proteins (20 μg) were separated by 10% SDS-PAGE followed by transfer to a polyvinylidene fluoride transfer membrane (Merck, Amsterdam, The Netherlands). Membranes were blocked for 1 h at room temperature in Tris-buffered saline tween-20 buffer with 5% non-fat dry milk followed by an overnight incubation with specific primary antibodies. Primary antibodies specific for cannabinoid type 1 receptor (CB1R), E2-F, AMPK, P-AMPK, ACC, P-ACC and tubulin were purchased from Cell Signaling (Leiden, The Netherlands). A primary antibody specific for uncoupling protein 1 (UCP1) was purchased from

Sigma-Aldrich. All antibodies were diluted 1:1000. Blots were incubated with horseradish peroxidase-conjugated secondary antibodies for 1 h at room temperature. Bands were visualized with SuperSignal West Pico Chemiluminescent Substrate (Pierce) and quantified using ImageJ (version 1.47).

Statistical analysis

All data are expressed as mean ± SEM. Statistical analysis using the unpaired two-tailed Student's test was performed with the SPSS 20.0 software package for Windows (SPSS, Chicago, United States) to determine differences between vehicle- and compound-treated groups. A P-value < 0.05 was considered statistically significant.

RESULTS

Systemic CB1R blockade by rimonabant in DIO mice reduces obesity and dyslipidemia and increases energy expenditure. To investigate the effect of systemic CB1R blockade on body composition and energy balance, E3L.CETP transgenic mice were fed a HFD for 12 weeks to render them obese (mean body weight: 53.2 ± 0.9 g) and treated with rimonabant or vehicle for 4 weeks. Rimonabant elicited a profound decrease in body mass (-25%, P<0.001; **FIGURE 1A)** which was not due to a decrease in lean mass but rather to a massive decrease in fat mass (-32%, P<0.001; **FIGURE 1B)**. Rimonabant decreased caloric intake transiently (i.e. until day 6) **(FIGURE 1C)**, in accordance with previous observations (35, 36), while it persistently induced weight loss throughout the treatment period (i.e. 4 weeks). Furthermore, rimonabant markedly diminished plasma TG levels (-59%, P<0.05) and TC levels (-40%, P<0.01) **(FIGURE 1D)**, which is in line with previous human studies (10-12). Rimonabant tended to reduce plasma phospholipid (PL) levels (-31%, P=0.05) and had no effect on plasma free fatty acid (FFA) levels. Lipoprotein profiling showed that the marked decrease in plasma TG mostly resulted from a reduction in VLDL-TG (AUC -62%) **(FIGURE 1E)**. The persistent reduction in body weight despite the transient decrease in food intake following rimonabant treatment suggests increased energy expenditure. Indeed, rimonabant increased substrate utilization reflected by increased fat oxidation (+18%, P<0.05; **FIGURE 1F)**, carbohydrate (CHO) oxidation (+18%, P<0.05; **FIGURE 1G)**, and consequently total energy expenditure (+17%, P<0.05; **FIGURE 1H)**, as measured via indirect calorimetry, without increasing locomotor activity **(FIGURE 1I)**.

Systemic CB1R blockade by rimonabant attenuates dyslipidemia by activating brown adipose tissue. Plasma VLDL-TG levels are determined by the balance between hepatic VLDL-TG production and VLDL-TG clearance by lipoprotein lipase (LPL)-expressing peripheral organs. Therefore, to gain insight into the mechanism by which systemic CB1R antagonism reduces plasma VLDL-TG, we first assessed the effect of rimonabant on VLDL production. DIO mice were treated with rimonabant or vehicle for 4 weeks and then sequentially injected with Trans[35]S and Triton WR1339 resulting in linear accumulation of VLDL in which newly synthe-
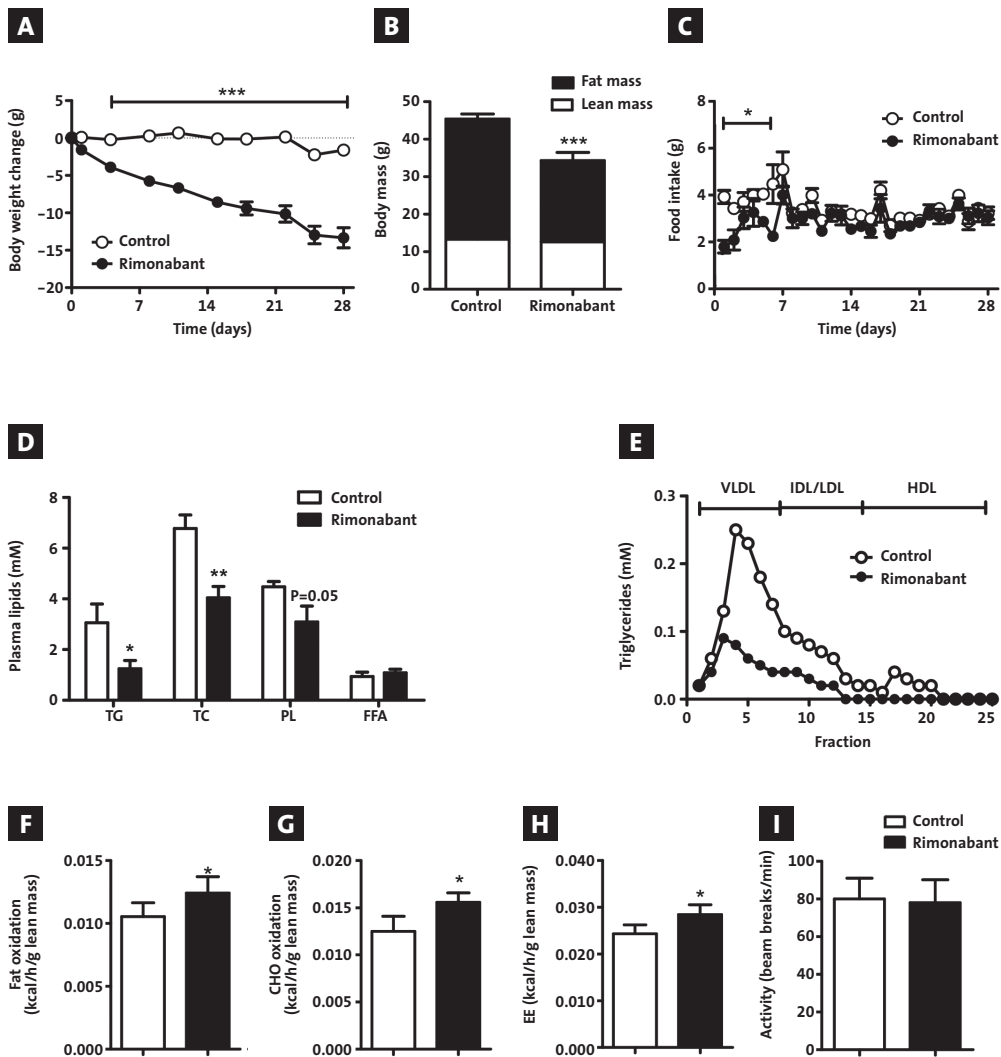
FIGURE 1 – Systemic CB1R blockade by rimonabant in DIO mice reduces obesity and dyslipidemia and increases energy expenditure. Male E3L.CETP mice were fed a HFD for 12 weeks to induce DIO and were then treated with rimonabant or vehicle for 4 weeks while housed at 21°C. **A** Body weight change (g) during the treatment period. **B** Lean and fat mass (g) as measured via DEXA-scan after 4 weeks of treatment. **C** Mean daily food intake (g) during the treatment period. **D** Plasma triglyceride (TG), total cholesterol (TC), phospholipid (PL), and free fatty acid (FFA) levels in 4-hour fasted mice after 4 weeks of treatment. **E** TG distribution over lipoproteins after separation from pooled plasma (n=9) by FPLC. **F** Fat oxidation, **G** carbohydrate (CHO) oxidation, **H** energy expenditure (EE), and **I** activity levels as measured during 5 consecutive days in the fourth week of treatment via fully automatic metabolic cages. **F-H** Measurements were corrected for lean mass. Values are means ± SEM (n=9) *P<0.05, **P<0.01, ***P<0.001 compared to the control group.

sized apolipoproteins are radiolabeled. Rimonabant did not affect the time-dependent accumulation of plasma TG following Triton injection **(FIGURE 2A)**. Therefore, the VLDL-TG production rate, as determined from the slope of the curve, was not significantly different. In addition, the rate of VLDL-apoB production did not change **(FIGURE 2B)**. In line with these observations, hepatic expression of lipogenic genes such as fatty acid synthase *(Fasn)* and stearoyl-CoA desaturase *(Scd1)* was unchanged **(FIGURE 2C)**. All together, these data demonstrate that global CB1R antagonism does not diminish dyslipidemia by lowering hepatic VLDL-TG production.

To investigate whether rimonabant increases VLDL-TG clearance, we determined the kinetics of i.v. injected [3H]TO-labeled TG-rich VLDL-like emulsion particles, which have been previously shown to mimic the metabolic behavior of TG-rich lipoproteins (30), and studied the plasma clearance and organ distribution of [3H]TO-derived fatty acids (FA) in mice treated with rimonabant or vehicle for 4 weeks. Rimonabant accelerated clearance of [3H]TO from plasma (t½ =3.9 ± 0.6 *vs.* 6.4 ± 0.4 min, P<0.05) **(FIGURE 2D)**, as explained by increased uptake of [3H]TO-derived activity by energy-dissipating BAT (+53%, P<0.05; **FIGURE 2E**). Of note, rimonabant decreased the uptake of [3H]TO by the energy-storing sWAT depot (-42%, P<0.05).

To further investigate the molecular mechanism by which systemic CB1R blockade increased FA uptake by BAT, the mRNA expression of genes involved in both BAT differentiation, BAT activity, TG lipolysis and FA uptake were determined. Rimonabant did not affect expression of genes involved in BAT differentiation *(Pgc1α, Prdm16)* and intracellular lipolysis *(Hsl, Atgl)* (data not shown). However, as shown in **FIGURE 2F,** rimonabant increased expression of *Lpl* (+30%, P<0.05) and *Cd36* (+24%, P<0.05) that drive extracellular VLDL-TG lipolysis and subsequent uptake of FA by BAT (18). In addition, rimonabant increased expression of *Ucp1,* which encodes the uncoupling protein that mediates thermogenesis (+49%, P<0.05). Furthermore, histology showed a more intense immunohistochemical staining of UCP-1 in BAT **(FIGURE 2G)** as well as a decrease in intracellular lipid droplet size, reflected by a decrease in relative lipid area (-39%, P<0.001; **FIGURE 2H**), both pointing to more active BAT (37). Thus, these data provide strong evidence that systemic CB1R antagonism diminishes dyslipidemia and increases energy expenditure, by promoting VLDL-TG uptake and subsequent combustion by BAT.

Systemic CB1R blockade by rimonabant diminishes TG storage in WAT and liver. To investigate whether the increased flux of TG towards BAT reduces (ectopic) TG accumulation, we analyzed WAT and the liver in more detail. Indeed, from the VLDL-TG clearance experiment it appeared that retention of [3H]TO-derived activity by the energy storing sWAT depot was diminished after rimonabant treatment (-42%, P<0.05; **FIGURE 2E**). In line with this, the cell size of white adipocytes was decreased in this depot as evident after H&E staining **(SUPPL. FIGURE 1A)**. In addition, rimonabant diminished expression of the lipogenic genes *Fasn* (-58%, P<0.05) and *Scd1* (-54%, P<0.05), while it increased expression of the lipolytic enzyme hormone sensitive lipase *(Hsl)* (+126%, P<0.05) in WAT **(SUPPL. FIGURE 1B)**, suggesting net FA efflux from WAT. In liver, rimonabant markedly decreased liver weight **(SUPPL. FIGURE 2A)**, which was
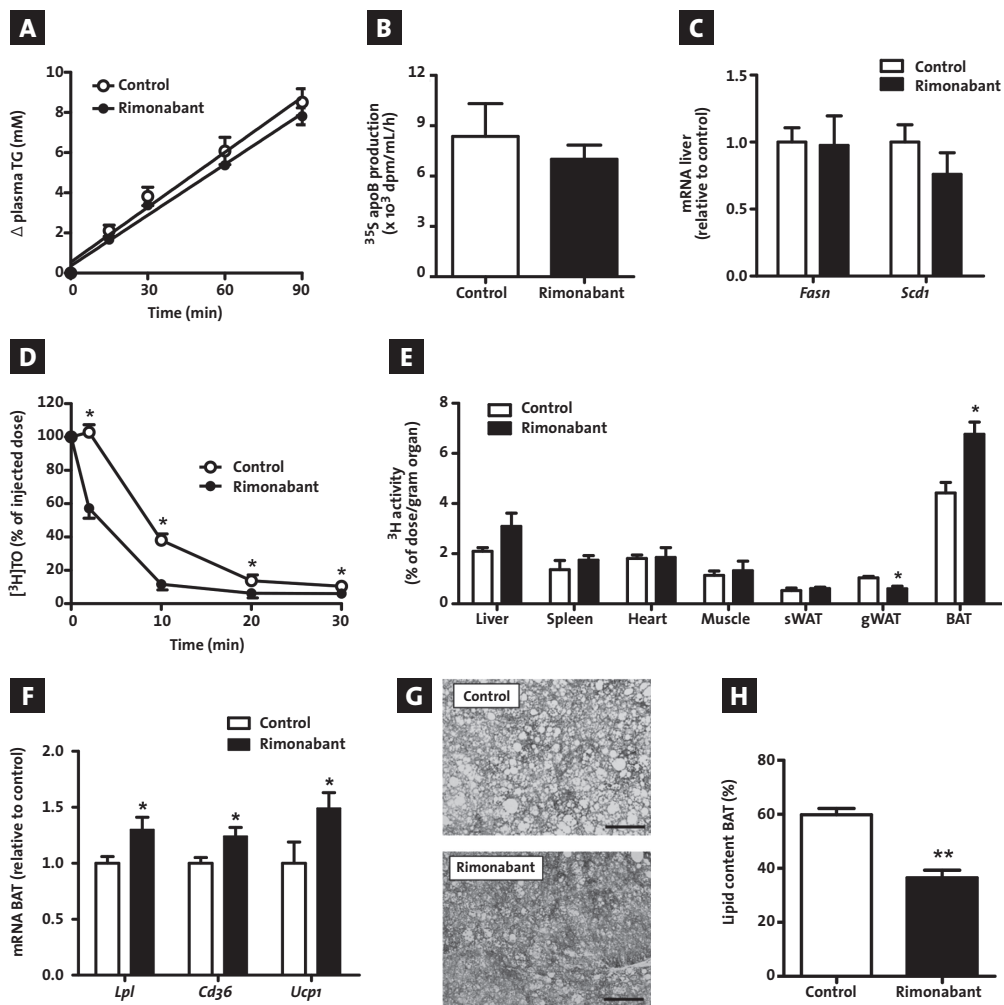
FIGURE 2 – Systemic CB1R blockade by rimonabant in DIO mice attenuates dyslipidemia by activating brown adipose tissue. Male E3L.CETP mice were fed a HFD for 12 weeks to induce DIO and were then treated with rimonabant or vehicle for 4 weeks while housed at 21°C **A** After 4 weeks of treatment, 4-hour fasted mice were injected intravenously with Tran[35S] and TritonWR1339 and blood samples were drawn at the indicated time points. TG concentrations were determined and plotted as the increase in plasma TG relative to t=0. **B** ApoB production rate, as measured by counting 35S-activity in the VLDL fraction isolated after 90 min. **C** Expression of *Fasn* and *Scd1* in liver as measured by qRT-PCR. **D** After 4 weeks of treatment, 4-hour fasted mice were injected intravenously with [3H]TO-labeled VLDL-like emulsion particles, blood was collected at the indicated time points and radioactivity was measured in plasma. **E** Uptake of [3H]TO-derived radioactivity by various organs was determined, and expressed as percentage of the injected dose per gram wet tissue weight. **F** Expression of *Lpl, Cd36,* and *Ucp1* in BAT as measured by qRT-PCR. **G** Representative pictures of immunohistochemical UCP-1 stainings of BAT in vehicle (top) and rimonabant (bottom) treated mice. Pictures were taken at 100x magnification (scale bar 100 μm). **H** Percentual lipid content in BAT tissue sections as quantified by use of ImageJ.

Values are means ± SEM (n=9) and expression of genes was corrected for the housekeeping genes ß2-microgulobulin and 36b4. *P<0.05, ***P<0.001 compared to the control group.
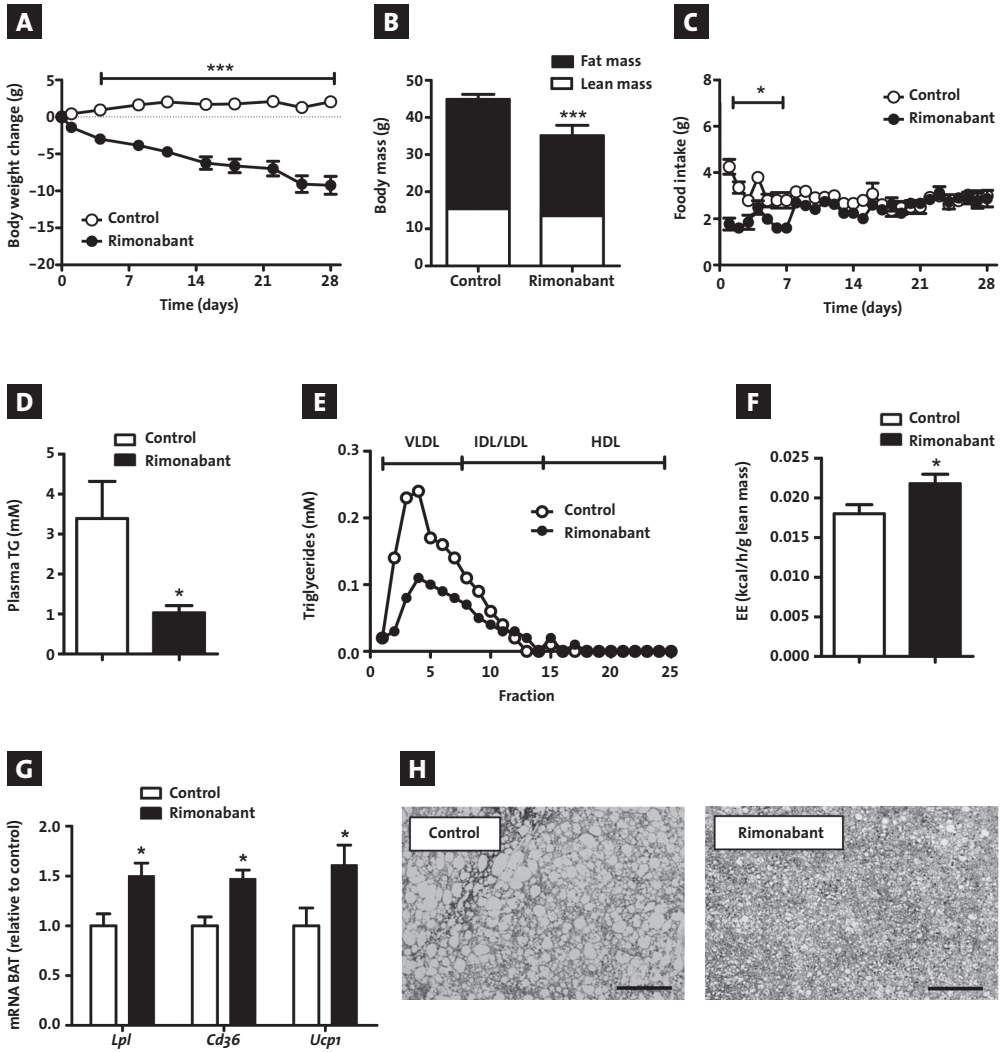
FIGURE 3 – The anti-obesity and lipid-lowering effects of systemic CB1R blockade by rimonabant in DIO mice are not abrogated at thermoneutrality. Male E3L.CETP mice were fed a HFD for 12 weeks to induce DIO and were then treated with rimonabant or vehicle for 4 weeks while housed at 28°C **A**. Body weight change (g) during the treatment period. **B** Lean and fat mass (g) as measured via DEXA-scan after 4 weeks of treatment. **C** Mean daily food intake (g) during the treatment period. **D** Plasma triglyceride (TG) levels in 4-hour fasted mice after 4 weeks of treatment. **E** TG distribution over lipoproteins after separation from pooled plasma (n=9 per group) by FPLC. **F** Energy expenditure (EE) as measured during 5 consecutive days in the fourth week of treatment via fully automatic metabolic cages, corrected for lean mass. **G** Expression of *Lpl, Cd36,* and *Ucp1* in BAT as measured by qRT-PCR **H** Representative pictures of immunohistochemical UCP-1 stainings of BAT in vehicle (left) and rimonabant (right) treated animals. Pictures were taken at 100x magnification (scale bar 100 µm).

Values are means ± SEM (n=9) *P<0.05, ** P<0.01, ***P<0.001 compared to the control group.

accompanied by a reduction in liver TG content (-45%, P<0.01) **(SUPPL. FIGURE 2B)** and smaller intracellular lipid vacuoles **(SUPPL. FIGURE 2C)**. Furthermore, rimonabant caused a (likely compensatory) downregulation of hepatic expression of genes involved in lipid oxidation, such as acyl-CoA synthetase long-chain family member 1 *(Acsl1)* and acetyl-CoA carboxylase 2 *(Acc2)* **(SUPPL. FIGURE 2D)**, while genes involved in lipogenesis were not affected **(FIGURE 2C)**. Thus, these data suggest that systemic CB1R blockade reduces storage of TG in WAT and liver, which may, at least in part, be a consequence of increased FA demand and flux towards BAT.

The anti-obesity and lipid-lowering effects of systemic CB1R blockade by rimonabant are not abrogated at thermoneutrality. BAT is densely innervated by the sympathetic nervous system (SNS) (19). Therefore, one of the mechanisms by which systemic CB1R blockade may lead to BAT activation could involve central CB1R blockade resulting in increased sympathetic outflow towards BAT. To investigate whether rimonabant acts centrally by increasing sympathetic nervous system (SNS) activation towards BAT, we next evaluated the effects of rimonabant in DIO mice that were housed at thermoneutral temperature (28°C). At thermoneutrality, rimonabant still markedly reduced obesity **(FIGURE 3A-B)** without affecting lean mass. This was accompanied by a transient decrease in food intake (i.e. until day 6) **(FIGURE 3C)**. Importantly, at thermoneutrality rimonabant still lowered plasma TG (-70%, P<0.05; **FIGURE 3D)**, which was mainly due to a reduction in VLDL-TG (AUC -52%; **FIGURE 3E)**. Furthermore, rimonabant still increased whole-body fat and carbohydrate oxidation **(SUPPL. FIGURE 3A-B)**, resulting in increased total energy expenditure (+21%, P<0.05; **FIGURE 3F)**, accompanied by increased markers of BAT activation both on mRNA **(FIGURE 3G)** and histological levels **(FIGURE 3H)**. Thus, these data suggest that the reduction in dyslipidemia, increase in energy expenditure and activation of BAT by systemic CB1R blockade occurs at least in part independent of SNS activation of BAT.

In vitro CB1R blockade by rimonabant induces activation of brown adipocytes and stimulation of AMPK phosphorylation. To explore the possibility that direct blockade of a CB1R in BAT may be responsible for the anti-obesity and lipid-lowering effect induced by systemic CB1R blockade, we first investigated whether the CB1R is expressed on BAT. Indeed, western blots on protein from tissues derived from untreated mice showed that the CB1R is highly expressed in BAT **(FIGURE 4A)**, even when compared to the expression in hypothalamus and liver. Furthermore, *in vitro* treatment of T37i brown adipocytes with rimonabant dose-dependently increased glycerol release **(FIGURE 4B)**, pointing to increased intracellular lipolysis, and upregulated UCP-1 protein **(FIGURE 4C)**. AMP-activated protein kinase (AMPK) serves as an intracellular energy sensor and activation of AMPK by means of phosphorylation results in enhanced fatty acid and glucose oxidation in a variety of tissues (38). Of note, CB1R blockade has been shown to increase AMPK phosphorylation in both liver cells (39) and white adipocytes (40). In line with this, we found that *in vitro* treatment of cultured T37i brown adipocytes with rimonabant induced AMPK phosphorylation **(FIGURE 4D)** as well as phosphorylation of ACC **(FIGURE 4E)**, the downstream effector of AMPK.

Altogether, these data indicate that direct blockade of the CB1R on brown adipocytes directly stimulates their activity with respect to intracellular lipolysis and UCP-1 protein content, accompanied by enhanced phosphorylation of AMPK and ACC.

Strictly peripheral CB1R blockade by AM6545 reduces obesity and dyslipidemia and increases energy expenditure in DIO mice. To investigate whether peripheral CB1R blockade is sufficient to induce weight loss and reverse dyslipidemia *in vivo,* we treated DIO mice for four weeks with vehicle or AM6545, a peripherally restricted CB1R antagonist that has been previously shown not to elicit central side effects (17). AM6545 markedly reduced body weight (-19%, P<0.001; **FIGURE 5A)** and fat mass (-23%, P<0.01; **FIGURE 5B)**, without altering lean

7
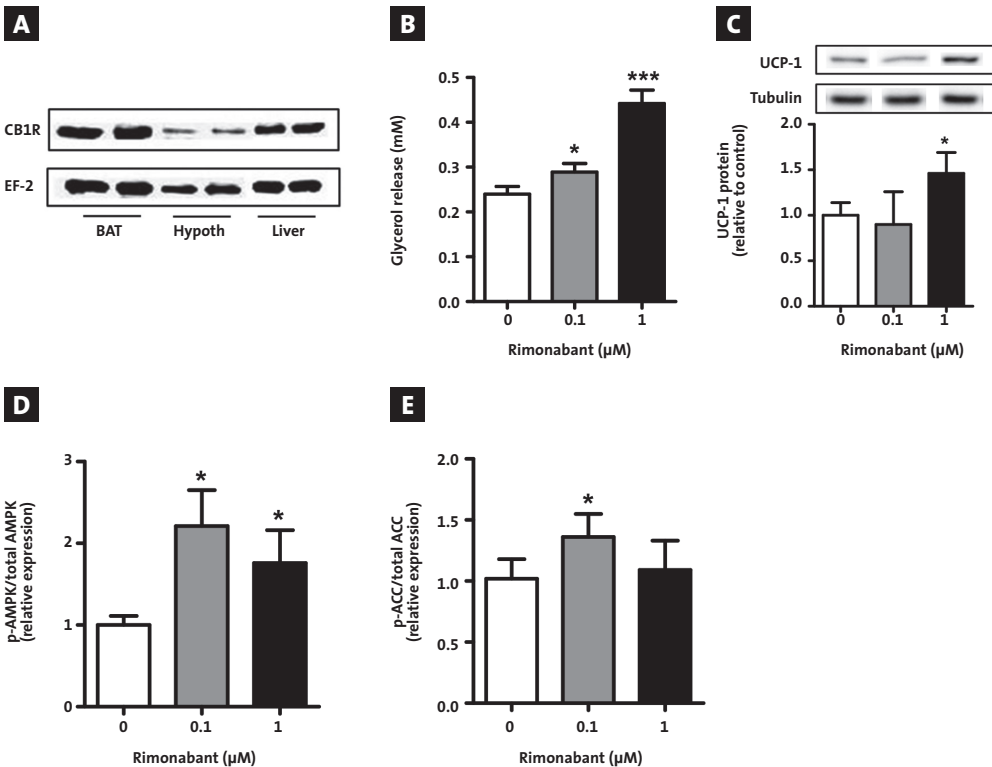
FIGURE 4 – Rimonabant directly stimulates BAT activity in T37i brown adipocytes in vitro. **A** CB1R protein expression was measured via western blot in BAT, hypothalamus and liver derived from diet-induced obese E3L.CETP transgenic mice with elongation factor 2 (EF-2) as housekeeping protein. **B-F** T37i brown adipocytes were treated with rimonabant (0, 0.1 or 1 µM) for 8 hours and **B** glycerol release was measured in the supernatant, and protein content of (C) UCP-1, (D) p-AMPK/AMPK **E** p-ACC/ACC and **F** Pgc1α was measured via western blot. Tubulin was used as housekeeping protein.

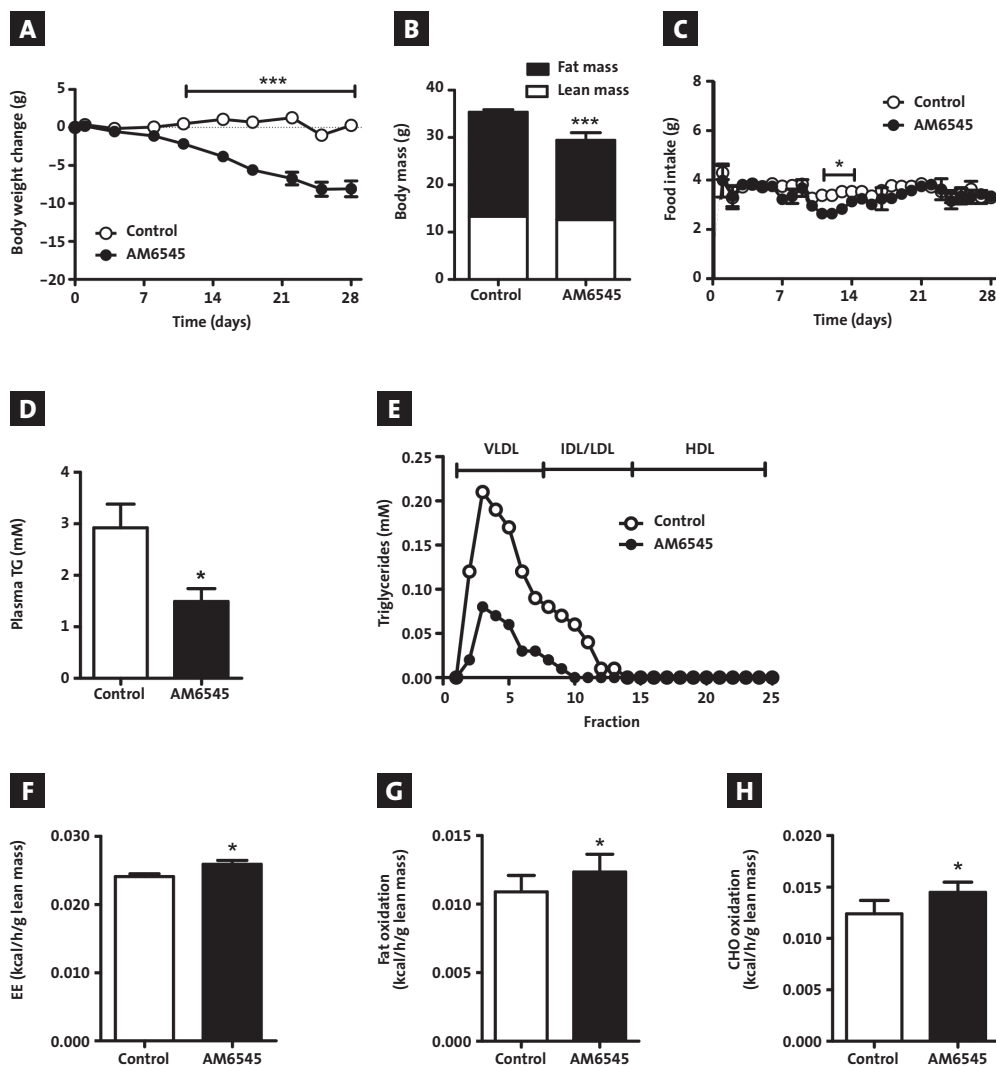Values are means ± SD (n=3) *P<0.05, ***P<0.001 compared to the control group.

FIGURE 5 – Strictly peripheral CB1R blockade by AM6545 reduces obesity and dyslipidemia and increases energy expenditure in DIO mice. Male E3L.CETP mice were fed a HFD for 12 weeks to induce DIO and were then treated with AM6545 or vehicle for 4 weeks while housed at 21°C. **A** Body weight change (g) during the treatment period. **B** Lean and fat mass (g) as measured via DEXA-scan after 4 weeks of treatment. **C** Mean daily food intake (g) during the treatment period. **D** Plasma triglyceride (TG) levels in 4-hour fasted mice after 4 weeks of treatment. **E** TG distribution over lipoproteins after separation from pooled plasma (n=9 per group) by FPLC. **F-H** energy expenditure, fat oxidation and carbohydrate (CHO) oxidation as measured during 5 consecutive days in the fourth week of treatment via fully automatic metabolic cages, corrected for lean mass. Values are means ± SD (n=9) *P<0.05, ***P<0.001 compared to the control group.
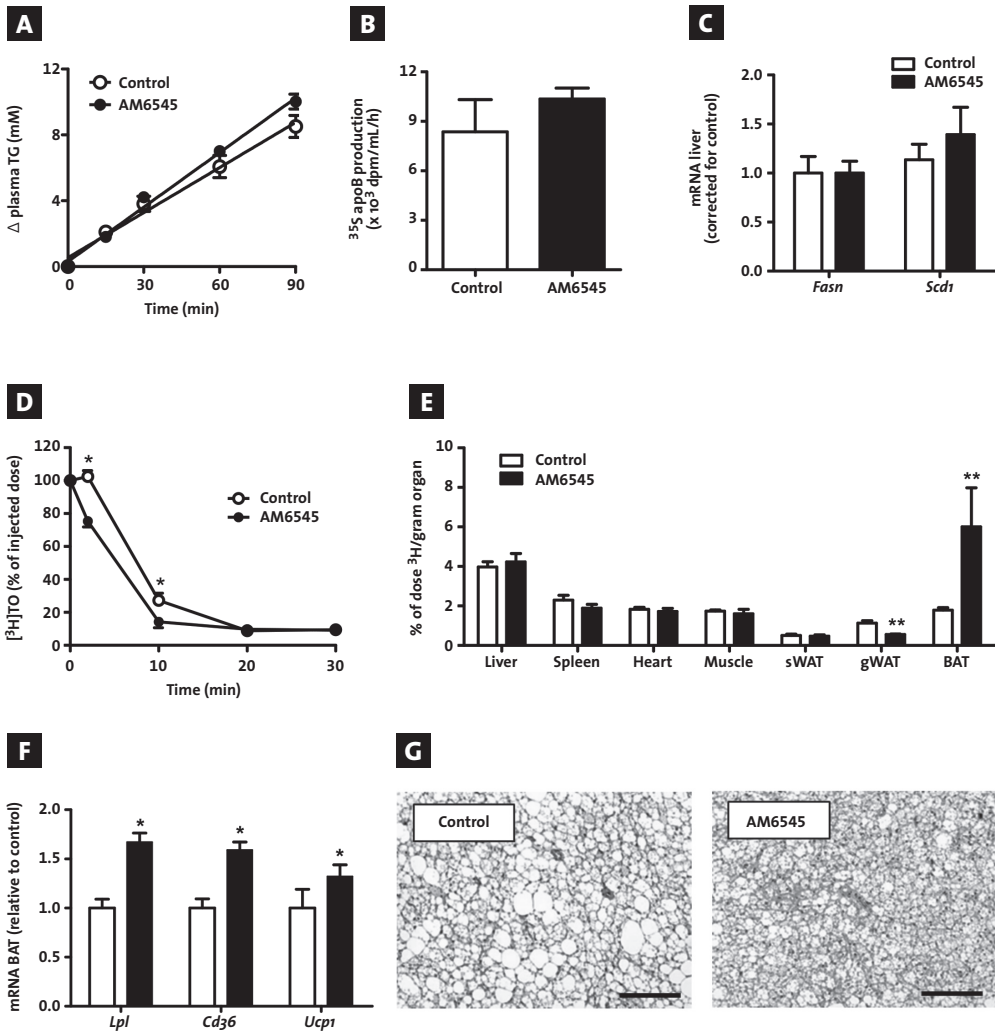
FIGURE 6 – Strictly peripheral CB1R blockade by AM6545 attenuates dyslipidemia in DIO mice by activating brown adipose tissue. Male E3L.CETP mice were fed a HFD for 12 weeks to induce DIO and were then treated with AM6545 or vehicle for 4 weeks while housed at 21°C. **A** After 4 weeks of treatment, 4-hour fasted mice were injected intravenously with Tran[35S] and TritonWR1339 and blood samples were drawn at the indicated time points. TG concentrations were determined and plotted as the increase in plasma TG relative to t=0. **B** ApoB production rate, as measured by counting [35S]-activity in the VLDL fraction after 90 min. **C** Expression of *Fasn* and *Scd1* in liver as measured by qRT-PCR. **D** After 4 weeks of treatment, 4-hour fasted mice were injected intravenously with [3H]TO-labeled VLDL-like emulsion particles. Blood was collected at the indicated time points and radioactivity was measured in plasma. **E** Uptake of [3H]TO-derived radioactivity by various organs, and expression per gram wet tissue weight. **F** Expression of *Lpl*, *Cd36*, and *Ucp1* in BAT as measured by qRT-PCR. (G) Representative pictures of immunohistochemical UCP-1 stainings of BAT in vehicle (left) and rimonabant (right) treated animals. Pictures were taken at 100x magnification (scale bar 100 μm).

Values are means ± SEM (n=9) and expression of genes was corrected for the housekeeping genes ß2-microglobulin and 36b4. *P<0.05, **P<0.01, ***P<0.001 compared to the control group.

mass. AM6545 did not induce the initial transient decrease in food intake as seen with rimonabant, although a slight decrease was evident later during the treatment period **(FIGURE 5C)**. However, total caloric intake was not affected. Furthermore, AM6545 substantially decreased plasma TG levels (-49%, P<0.05; **FIGURE 5D)**, which mostly resulted from a reduction in VLDL-TG (AUC -73%; **FIGURE 5E)**. In addition, AM6545 increased total energy expenditure **(FIGURE 5F)**, which was due to an increase in both fat and carbohydrate oxidation **(FIGURE 5G-H)**. Thus, these data demonstrate that peripheral CB1R blockade is sufficient to diminish obesity and dyslipidemia in DIO.

Strictly peripheral CB1R blockade by AM6545 attenuates dyslipidemia by activating brown adipose tissue. To investigate whether peripheral CB1R blockade also diminished dyslipidemia by increasing FA uptake by BAT, we again assessed VLDL-TG production and clearance. Just like rimonabant, AM6545 did not affect the production rates of VLDL-TG and VLDL-apoB **(FIGURE 6A-B)** or hepatic expression of lipogenic genes **(FIGURE 6C)**. Instead, AM6545 also accelerated clearance of [3H]TO-labeled VLDL-like emulsion particles from plasma **(FIGURE 6D)**, accompanied by a marked increase of 3H retention by BAT (+235%, P<0.01; **FIGURE 6E)**, and a decrease in 3H uptake by sWAT (-51%, P<0.01). In BAT, AM6545 increased expression of *Lpl* (+67%,P<0.05), *Cd36* (+59%, P<0.05) and *Ucp1* (+32%, P<0.05; **FIGURE 6F)** and decreased lipid content **(FIGURE 6G)**, all pointing to increased BAT activity. AM6545 also decreased white adipocyte size **(SUPPL. FIGURE 4A)** and liver weight (-24%, P<0.001; **SUPPL. FIGURE 4B)** accompanied by a reduction in liver TG content (-17%, P<0.05) **(SUPPL. FIGURE 4C)** and lipid vacuole size **(SUPPL. FIGURE 4D)**. Thus, peripheral CB1R blockade is sufficient to diminish dyslipidemia, and probably also obesity, by promoting VLDL-TG uptake and subsequent combustion of engulfed FA by BAT.

DISCUSSION

Systemic CB1R blockade by the inverse CB1R agonist rimonabant alleviates the excess body weight and dyslipidemia that are associated with obesity, both in mice and in humans (8-12). In this study, we demonstrate that systemic CB1R blockade reverses DIO and reduces plasma VLDL-TG by selectively increasing VLDL-TG clearance by metabolically active BAT followed by combustion. Of note, the mechanism involves peripheral activation of BAT since the effects were still present at thermoneutrality and could be recapitulated by using the strictly peripheral (17) CB1R antagonist AM6545. Accordingly, cultured brown adipocytes could be activated by blockade of the CB1R with rimonabant.

Systemic CB1R blockade by rimonabant resulted in massive activation of BAT, as evidenced by reduced lipid content and increased UCP-1 expression, accompanied by increased energy expenditure, which is in accordance with previous studies (36,41). Of note, by performing kinetic studies with radioactively labeled VLDL-TG we provided clear evidence that the TG-lowering effect of rimonabant is due to increased uptake of TG-derived FAs by BAT.

Since metabolically active BAT has been shown to be present and active in human adults (20-23), it is tempting to speculate that the body weight-reducing and TG-lowering effects of rimonabant previously found in obese subjects might be due to activation of BAT, although the precise role of BAT in TG metabolism in humans remains to be established.

Previous studies suggested central CB1R blockade as the main mechanism by which rimonabant induces BAT activation, resulting in increased sympathetic outflow towards BAT and increased energy expenditure (36,41). For instance, Bajzer and colleagues (36) reported that denervation of BAT in mice blunted the effect of rimonabant on insulin-mediated glucose uptake. However, in their study, the increase in energy expenditure and the reduction in body weight and fat mass were not blunted by BAT denervation, suggesting that a peripheral mechanism is at least in part involved in these beneficial effects. Indeed, we found that treatment of DIO mice with the strictly peripheral CB1R antagonist AM6545 still resulted in increased energy expenditure accompanied by increased uptake of TG-derived FAs by BAT as well as significant weight loss and reduction in dyslipidemia. Furthermore, we showed that the CB1R is highly expressed in BAT, and rimonabant increased the activity of brown adipocytes, further supporting the possibility of a peripheral mode of action of CB1R blockade in BAT.

We found that systemic blockade of the CB1R by rimonabant did not affect VLDL-TG production following either systemic or selective peripheral CB1R blockade. In contrast, a study by Tam and colleagues (17) reported that blocking the peripheral CB1R by AM6545 treatment resulted in a marked increase in the production of VLDL-TG in both DIO C57Bl/6 and leptin-deficient ob/ob mice. This might be explained by differences in study set-up, since Tam and colleagues measured VLDL-TG production after 1 week of treatment while in the present study VLDL-TG production was measured after 4 weeks. Likely, CB1R blockade transiently increases VLDL-TG production, leading to a fast initial reduction in hepatic steatosis as was also observed in their study. The subsequent normalization in VLDL production that we found in our study after 4 weeks of treatment may then be the consequence of a lower supply of FFAs towards the liver for incorporation into VLDL-TG, since these are efficiently cleared by BAT.

While we provide clear evidence that the TG-lowering effect of CB1R blockade is due to peripheral activation of BAT, the mechanism by which CB1R blockade lowers body weight and fat mass is less clear and no consistent mechanism has been reported up to date. Although BAT activation has been repeatedly shown to decrease body weight and fat mass (18,42,43), we cannot exclude that CB1R blockade on peripheral tissues other than BAT may contribute to the weight-reducing effect. For instance, the CB1R has been shown to be present on white adipocytes (16) and treatment of mice with rimonabant and AM6545 increased lipolysis (17,44,45). Accordingly, we also found that rimonabant increased mRNA expression of *Hsl* in subcutaneous WAT. Furthermore, the weight-reducing effect of global CB1R blockade is also at least in part due to an initial transient decrease in food intake induced by rimonabant. The greater efficacy of rimonabant over AM6545 in reducing body weight is then likely explained by the fact that AM6545 did not affect total caloric intake over the treatment period, as has been shown before (17). Thus, future studies are needed to

elucidate the specific contribution of BAT in the weight-reducing effect of (peripheral) CB1R blockade.

The intracellular mechanism by which CB1R blockade is linked to BAT thermogenesis likely involves phosphorylation of AMP-activated kinase (AMPK), a key evolutionary conserved cellular energy sensor that regulates metabolism (37). We show that CB1R blockade resulted in increased AMPK phosphorylation in brown adipocytes, which is in accordance with previous studies performed in hepatocytes (39) and white adipocytes (40). Thus, AMPK might be a central player by which CB1R blockade results in BAT activation. Future studies should be directed at investigating these pathways in more detail.

Together, our study shows that CB1R blockade diminishes dyslipidemia by inducing BAT-mediated VLDL-TG uptake and BAT thermogenesis via a peripheral mode of action. Our data suggest that blockade of the peripheral CB1R in BAT may be a promising therapy to combat obesity and to lower cardiovascular risk without inducing centrally mediated side effects.

7

ACKNOWLEDGEMENTS

REFERENCES

1   Pagotto, U., Marsicano, G., Cota, D., Lutz, B., and Pasquali, R. (2006) The emerging role of the endocannabinoid system in endocrine regulation and energy balance. *Endocr Rev.* **27,** 73-100.

2   Piomelli, D. (2003) The molecular logic of endocannabinoid signalling. *Nat Rev Neurosci.* **4,** 873-884.

3   De Petrocellis, L., Cascio, M.G., and Di Marzo, V. (2004) The endocannabinoid system: a general view and latest additions. *Br J Pharmacol.* **141,** 765–774.

4   Howlett, A.C., Barth, F., Bonner, T.I., Cabral, G., Casellas, P., Devane, W.A., Felder, C.C., Herkenham, M., Mackie, K., Martin, B.R., Mechoulam, R., and Pertwee, R.G. (2002) International Union of Pharmacology. XXVII. Classification of cannabinoid receptors. *Pharmacol Rev.* **54,** 161–202.

5   Ravinet-Trillou, C., Delgorge, C., Menet, C., Arnone, M., and Soubrié, P. (2004) CB1 cannabinoid receptor knockout in mice leads to leanness, resistance to diet-induced obesity and enhanced leptin sensitivity. *Int J Obes Relat Metab Disord.* **28,** 640–648.

6   Engeli, S., Böhnke, J., Feldpausch, M., Gorzelniak, K. Janke, J., Bátkai, S., Pacher, P., Harvey-White, J., Luft, F.C., Sharma, A.M., and Jordan, J. (2005) Activation of the peripheral endocannabinoid system in human obesity. *Diabetes* **54,** 2838–2843.

7   Blüher, M., Engeli, S., Klöting, N., Berndt, J., Fasshauer, M., Bátkai, S., Pacher, P., Schön, M.R., Jordan, J., and Stumvoll, M. (2006) Dysregulation of the peripheral and adipose tissue endocannabinoid system in human abdominal obesity. *Diabetes.* **55,** 3053–3060.

8   Ravinet Trillou, C., Arnone, M., Delgorge, C., Gonalons, N., Keane, P., Maffrand, J.P., and Soubrie, P. (2003) Anti-obesity effect of SR141716, a CB1 receptor antagonist, in diet-induced obese mice. *Am J Physiol Regul Integr Comp Physiol.* **284,** R345–R353.

9   Gary-Bobo, M., Elachouri, G., Gallas, J.F., Janiak, P., Marini, P., Ravinet-Trillou, C., Chabbert, M., Cruccioli, N., Pfersdorff, C., Roque, C., Arnone, M., Croci, T., Soubrié, P., Oury-Donat, F., Maffrand, J.P., Scatton, B., Lachèretz, F., Le Fur, G., Herbert, J.M., and Bensaid, M. (2007) Rimonabant reduces obesity-associated hepatic steatosis and features of metabolic syndrome in obese Zucker fa/fa rats. *Hepatology* **46,** 122–129.

10 Van Gaal, L.F., Rissanen, A.M., Scheen, A.J., Ziegler, O., and Rossner, S. (2005) Effects of the cannabinoid-1 receptor blocker rimonabant on weight reduction and cardiovascular risk factors in overweight patients: 1-year experience from the RIO-Europe study. *Lancet* **365,** 1389–1397.

11 Despres, J.P., Golay, A., and Sjostrom, L. (2005) Effects of rimonabant on metabolic risk factors in overweight patients with dyslipidemia. *N Engl J Med.* **353,** 121–2134.

12 Pi-Sunyer, F.X., Aronne, L.J., Heshmati, H.M., Devin, J., and Rosenstock, J. (2006) Effect of rimonabant, a cannabinoid-1 receptor blocker, on weight and cardiometabolic risk factors in overweight or obese patients: RIONorth America: a randomized controlled trial. *JAMA* **295,** 761–775.

13 Addy, C., Wright, H., Van Laere, K., Gantz, I., Erondu, N., Musser, B.J., Lu, K., Yuan, J., Sanabria-Bohórquez, S.M., Stoch, A., Stevens, C., Fong, T.M., De Lepeleire, I., Cilissen, C., Cote, J., Rosko, K., Gendrano, I.N. 3rd, Nguyen, A.M., Gumbiner, B., Rothenberg, P., de Hoon, J., Bormans, G., Depré, M., Eng, W.S., Ravussin, E., Klein, S., Blundell, J., Herman, G.A., Burns, H.D., Hargreaves, R.J., Wagner, J., Gottesdiener, K., Amatruda, J.M., and Heymsfield, S.B. (2008) The acyclic cb1r inverse agonist taranabant mediates weight loss by increasing energy expenditure and decreasing caloric intake. *Cell Metab.* **7,** 68–78.

14 Osei-Hyiaman, D., DePetrillo, M., Pacher, P., Liu, J., Radaeva, S., Bátkai, S., Harvey-White, J., Mackie, K., Offertáler, L., Wang, L., and Kunos, G. (2005) Endocannabinoid activation at hepatic CB1 receptors stimulates fatty acid synthesis and contributes to diet-induced obesity. *J Clin Invest.* **115,** 1298–1305.

7

15 Eckardt, K., Sell, H., Taube, A., Koenen, M., Platzbecker, B., Cramer, A., Horrighs, A., Lehtonen, M., Tennagels, N., and Eckel, J. (2009) Cannabinoid type 1 receptors in human skeletal muscle cells participate in the negative crosstalk between fat and muscle. *Diabetologia* **52,** 664–674.

16 Cota, D., Marsicano, G., Tschöp, M., Grübler, Y., Flachskamm, C., Schubert, M., Auer, D., Yassouridis, A., Thöne-Reineke, C., Ortmann, S., Tomassoni, F., Cervino, C., Nisoli, E., Linthorst, AC., Pasquali, R., Lutz, B., Stalla, G.K., and Pagotto, U. (2003) The endogenous cannabinoid system affects energy balance via central orexigenic drive and peripheral lipogenesis. *J Clin Invest*. **112,** 423–431.

17 Tam, J., Vemuri, V.K., Liu, J., Bátkai, S., Mukhopadhyay, B., Godlewski, G., Osei-Hyiaman, D., Ohnuma, S., Ambudkar, S.V., Pickel, J., Makriyannis, A., and Kunos, G. (2010) Peripheral CB1 cannabinoid receptor blockade improves cardiometabolic risk in mouse models of obesity. *J Clin Invest*. **120,** 2953-2966.

18 Bartelt, A., Bruns, O.T., Reimer, R., Hohenberg, H., Ittrich, H., Peldschus, K., Kaul, M.G., Tromsdorf, U.I., Weller, H., Waurisch, C., Eychmüller, A., Gordts, P.L., Rinninger, F., Bruegelmann, K., Freund, B., Nielsen, P., Merkel, M., and Heeren, J. (2011) Brown adipose tissue activity controls triglyceride clearance. *Nat Med*. **17,** 200-205.

19 Cannon, B., and Nedergaard, J. (2004) Brown adipose tissue: function and physiological significance. *Physiol Rev*. **84,** 277-359.

20 Cypess, A.M., Lehman, S., Williams, G., Tal, I., Rodman, D., Goldfine, A.B., Kuo, F.C., Palmer, E.L., Tseng, Y.H., Doria, A., Kolodny, G.M., and Kahn, C.R. (2009) Identification and importance of brown adipose tissue in adult humans. *N Engl J Med*. **360,** 1509-1517.

21 Virtanen, K.A., Lidell, M.E., Orava, J., Heglind, M., Westergren, R., Niemi, T., Taittonen, M., Laine, J., Savisto, N.J., Enerbäck, S., and Nuutila, P. (2009) Functional brown adipose tissue in healthy adults. *N Engl J Med*. **360,** 1518-1525.

22 van Marken Lichtenbelt, W.D., Vanhommerig, J.W., Smulders, N.M., Drossaerts, J.M., Kemerink, G.J., Bouvy, N.D., Schrauwen, P., and Teule, G.J. (2009) Cold-activated brown adipose tissue in healthy men. *N Engl J Med*. **360,** 1500-1508.

23 Bakker, L.E.H., Boon, M.R., Van der Linden, R.A.D., Pereira Aris-Bouda, L., Van Klinken, J.B., Smit, F., Verberne, H.J., Jukema, J.W., Tamsma, J.T., Havekes, L.M., Van Marken Lichtenbelt, W.D., Jazet, I.M., and Rensen, P.C.N. (2013) Brown adipose tissue volume in healthy lean south Asian adults compared with white Caucasians: a prospective, case-controlled observational study. *The Lancet Diabetes and Endocrinology,* in press.

24 Westerterp, M., van der Hoogt, C.C., de Haan, W., Offerman, E.H., Dallinga-Thie, G.M., Jukema, J.W., Havekes, L.M., and Rensen, P.C. (2006) Cholesteryl ester transfer protein decreases high-density lipoprotein and severely aggravates atherosclerosis in APOE*3-Leiden mice. *Arterioscler Thromb Vasc Biol* **26,** 2552-2559.

25 de Haan, W., van der Hoogt, C.C., Westerterp, M., Hoekstra, M., Dallinga-Thie, G.M., Princen, H.M., Romijn, J.A., Jukema, J.W., Havekes, L.M., and Rensen, P.C. (2008) Atorvastatin increases HDL cholesterol by reducing CETP expression in cholesterol-fed APOE*3-Leiden.CETP mice. *Atherosclerosis*. **197,** 57-63.

26 van der Hoogt, C.C., de Haan, W., Westerterp, M., Hoekstra, M., Dallinga-Thie, G.M., Romijn, J.A., Princen, H.M., Jukema, J.W., Havekes, L.M., and Rensen, P.C. (2007) Fenofibrate increases HDL cholesterol by reducing the expression of the cholesteryl ester transfer protein. *J Lipid Res*. **48**, 1763-1771.

27 Van Klinken, J.B., Van den Berg, S.A.A., Havekes, L.M., and Willems van Dijk, K. (2012) Estimation of activity related energy expenditure and resting metabolic rate in freely moving mice from indirect calorimetry data. *PLoS One* **7,** e36162.

28 Feurer, I., and Mullen, J.L. (1986) Beside measurement of resting energy expenditure and respiratory quotient via indirect calorimetry. *Nutr Clin Prac*. **1,** 43-49.

7

29 Zambon, A., Hashimoto, S.I., and Brunzell, J.D. (1993) Analysis of techniques to obtain plasma for measurement of levels of free fatty acids. *J Lipid Res.* **34,** 1021-1028.

30 Rensen, P.C., van Dijk, M.C., Havenaar, E.C., Bijsterbosch, M.K., Kruijt, J.K., and van Berkel, T.J. (1995) Selective liver targeting of antivirals by recombinant chylomicrons--a new therapeutic approach to hepatitis B. *Nat Med.* **1,** 221-225.

31 Jong, M.C., Rensen, P.C., Dahlmans, V.E., van der Boom, H., van Berkel, T.J., and Havekes, L.M. (2001) Apolipoprotein C-III deficiency accelerates triglyceride hydrolysis by lipoprotein lipase in wild-type and apoE knockout mice. *J Lipid Res.* **42,** 1578-1585.

32 Redgrave, T.G., Roberts, D.C., and West, C.E. (1975) Separation of plasma lipoproteins by density-gradient ultracentrifugation. *Anal Biochem.* **65,** 42-49.

33 Bligh, E.G., and Dyer, W.J. (1959) A rapid method of total lipid extraction and purification. *Can J Biochem Physiol.* **37,** 911-917.

34 Zennaro, M.C., Le Menuet, D., Viengchareun, S., Walker, F., Ricquier, D., and Lombes, M. (1998) Hibernoma development in transgenic mice identifies brown adipose tissue as a novel target of aldosterone action. *J Clin Invest.* **101,** 1254–1260.

35 Hu, C., Wei, H., van den Hoek, A.M., Wang, M., van der Heijden, R., Spijksma, G., Reijmers, T.H., Bouwman, J., Wopereis, S., Havekes, L.M., Verheij, E., Hankemeier, T., Xu, G., and van der Greef, J. (2011) Plasma and liver lipidomics response to an intervention of rimonabant in ApoE*3Leiden. CETP transgenic mice. *PLoS One* **6,** e19423.

36 Bajzer, M., Olivieri, M., Haas, M.K., Pfluger, P.T., Magrisso, I.J., Foster, M.T., Tschöp, M.H., Krawczewski-Carhuatanta, K.A., Cota, D., and Obici, S. (2011) Cannabinoid receptor (CB1) antagonism enhances glucose utilisation and activates brown adipose tissue in diet-induced obese mice. *Diabetologia.* **54,** 3121-3131.

37 Hardie, D.G., Ross, F.A., and Hawley, S.A. (2012) AMPK: a nutrient and energy sensor that maintains energy homeostasis. *Nat Rev Mol Cell Biol.* **13,** 251-262.

38 Wu, H.M., Yang, Y.M., and Kim, S.G. (2011) Rimonabant, a cannabinoid receptor type 1 inverse agonist, inhibits hepatocyte lipogenesis by activating liver kinase B1 and AMP-activated protein kinase axis downstream of Gα i/o inhibition. *Mol Pharmacol.* **80,** 859-869.

39 Tedesco, L. (2008) Cannabinoid type 1 receptor blockade promotes mitochondrial biogenesis through endothelial nitric oxide synthase expression in white adipocytes. *Diabetes.* 57, 2028-2036.

40 Ortega-Molina, A., Efeyan, A., Lopez-Guadamillas, E., Muñoz-Martin, M., Gómez-López, G., Cañamero, M., Mulero, F., Pastor, J., Martinez, S., Romanos, E., Mar Gonzalez-Barroso, M., Rial, E., Valverde, A.M., Bischoff, J.R., and Serrano, M. (2012) Pten positively regulates brown adipose tissue function, energy expenditure and longevity. *Cell Metab.* **7,** 382-394.

41 Verty, A.N., Allen, A.M., and Oldfield, B.J. (2009) The effects of rimonabant on brown adipose tissue in rat: implications for energy expenditure. *Obesity (Silver Spring).* **17,** 254–261.

42 Tseng, Y.H., Kokkotou, E., Schulz, T.J., Huang, T.L., Winnay, J.N., Taniguchi, C.M., Tran, T.T., Suzuki, R., Espinoza, D.O., Yamamoto, Y., Ahrens, M.J., Dudley, A.T., Norris, A.W., Kulkarni, R.N., and Kahn, C.R. (2008) New role of bone morphogenetic protein 7 in brown adipogenesis and energy expenditure. *Nature.* **454,** 1000-1004.

43 Whittle, A.J., Carobbio, S., Martins, L., Slawik, M., Hondares, E., Vázquez, M.J., Morgan, D., Csikasz, R.I., Gallego, R., Rodriguez-Cuenca, S., Dale, M., Virtue, S., Villarroya, F., Cannon, B., Rahmouni, K., López, M., and Vidal-Puig, A. (2012) BMP8B increases brown adipose tissue thermogenesis through both central and peripheral actions. *Cell.* **149,** 871-885.

44 Jbilo, O., Ravinet-Trillou, C., Arnone, M., Buisson, I., Bribes, E., Péleraux, A., Pénarier, G., Soubrié, P., Le Fur, G., Galiègue, S., and Casellas, P. (2005) The CB1 receptor antagonist rimonabant reverses the diet-induced obesity phenotype through regulation of lipolysis and energy balance. *FASEB J.* **19,** 1567-1569.

7

45   Mølhøj, S., Hansen, H.S., Schweiger, M.,
     Zimmermann, R., Johansen, T., and Malmlöf, K.
     (2010) Effect of the cannabinoid receptor-1
     antagonist rimonabant on lipolysis in rats.
   *Eur J Pharmacol.* **646,** 38-45.

7

SUPPLEMENTARY APPENDIX
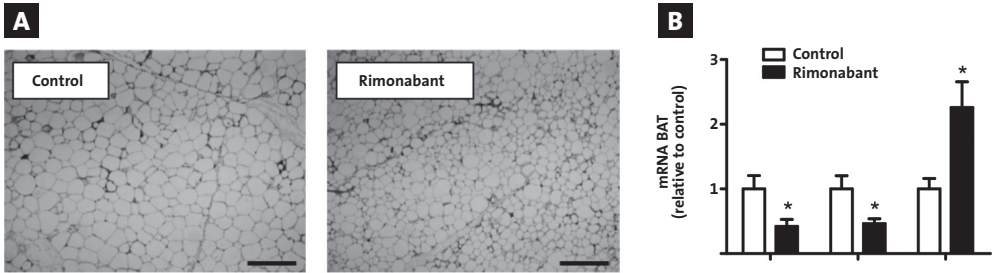
SUPPLEMENTARY FIGURE 1 – Effect of systemic CB1R blockade by rimonabant on subcutaneous WAT. Male E3L. CETP mice were fed a HFD for 12 weeks to induce diet-induced obesity and were then treated with rimonabant or vehicle for 4 weeks while being housed at an environmental temperature of 21°C. **A** Representative pictures of H&E stainings of sWAT in vehicle (left) and rimonabant (right) treated animals. Sections were enlarged 100x (scale bar 100 μm). **B** Expression of *Fasn, Scd1,* and *Hsl* in sWAT as measured by qRT-PCR.

Values are means ± SEM (n=9) and expression of genes was corrected for the housekeeping genes ß2-microglobulin and 36b4. *P<0.05 compared to the control group.
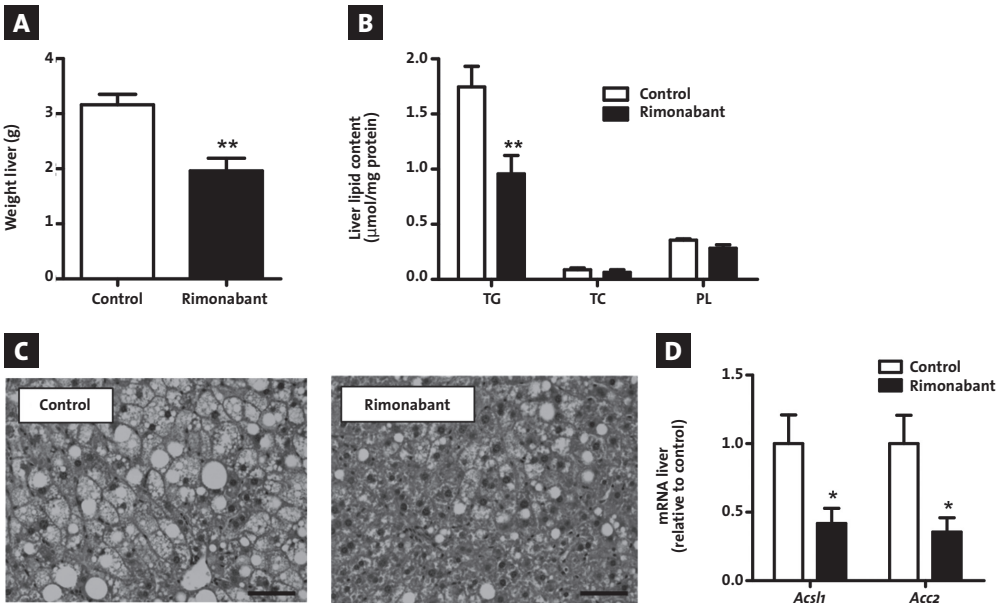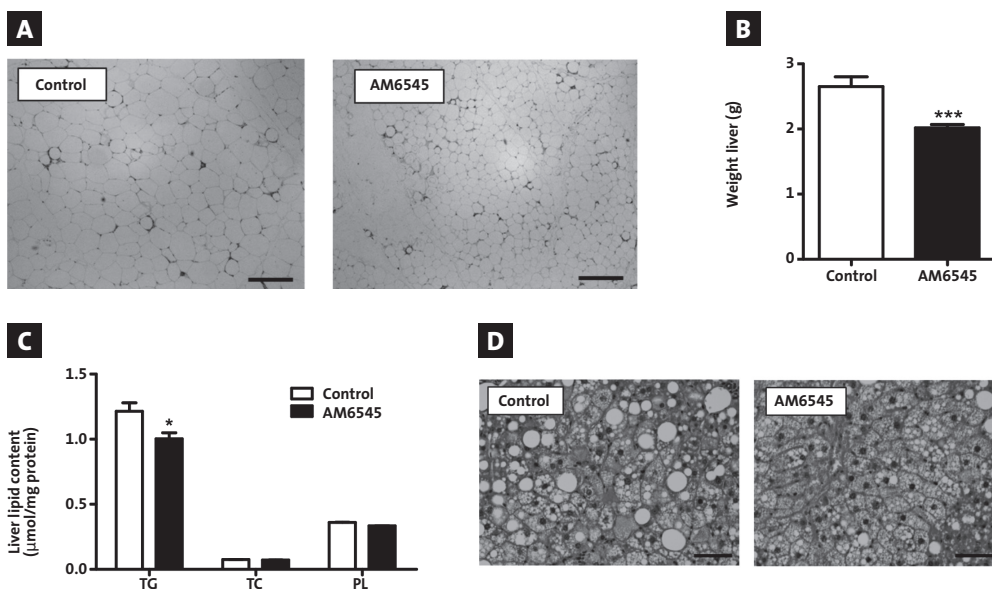

SUPPLEMENTARY FIGURE 2 – Effect of systemic CB1R blockade by rimonabant on hepatic steatosis. Male E3L. CETP mice were fed a HFD for 12 weeks to induce diet-induced obesity and were then treated with rimonabant or vehicle for 4 weeks while being housed at an environmental temperature of 21°C. **A** Liver weight (g). **B** Liver content of triglycerides (TG), total cholesterol (TC) and phospholipids (PL). **C** Representative pictures of H&E stainings of livers from vehicle (left) and rimonabant (right) treated animals. Pictures were taken at 100x magnification (scale bar 100 μm). **D** Expression of *Acsl1* and *Acc2* in liver as measured by qRT-PCR.

Values are means ± SEM (n=9) and expression of genes was corrected for the housekeeping genes ß2-microglobulin and 36b4. *P<0.05 , **P<0.01 compared to the control group.
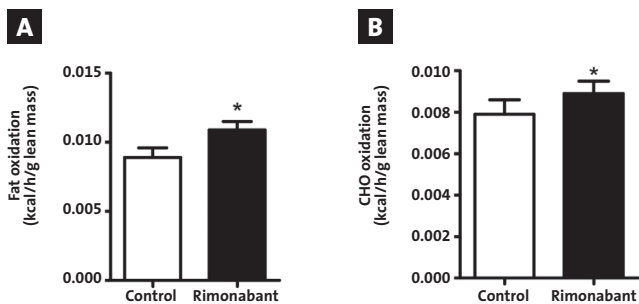
SUPPLEMENTARY FIGURE 3 – Systemic CB1R blockade increases fat and carbohydrate oxidation at thermo-neutrality. Male E3L.CETP mice were fed a HFD for 12 weeks to induce diet-induced obesity and were then treated with rimonabant or vehicle for 4 weeks while being housed at an environmental temperature of 28°C. **A-B** Fat and carbohydrate (CH) oxidation as measured during 5 consecutive days in the fourth week of treatment via fully automatic metabolic cages, corrected for lean body mass.

Values are means ± SEM (n=9). *P<0.05 compared to the control group.

SUPPLEMENTARY FIGURE 4 – Effect of strictly peripheral CB1R blockade by AM6545 on lipid storage in sWAT and liver. Male E3L.CETP mice were fed a HFD for 12 weeks to induce diet-induced obesity and were then treated with AM6545 or vehicle for 4 weeks while being housed at an environmental temperature of 21°C. **A** Representative pictures of H&E stainings of sWAT in vehicle (left) and AM6545 (right) treated animals. Pictures were taken at 100x magnification (scale bar 100 μm). **B** Liver weight (g). **C** Liver content of triglycerides (TG), total cholesterol (TC) and phospholipids (PL). **D** Representative pictures of H&E stainings of liver in vehicle (left) and AM6545 (right) treated animals. Pictures were taken at 100x magnification (scale bar 100 μm). Sections were enlarged 100x (scale bar 100 μm).

Values are means ± SEM (n=9). *P<0.05 , ***P<0.001 compared to the control group.